ACS ES&T Water

Open Access

pubs.acs.org/estwater

Article

Fluoro-Electrochemistry Based Phytoplankton Bloom Detection and Enumeration; Field Validation of a New Sensor for Ocean Monitoring

Samuel Barton,* Minjun Yang, Christopher Batchelor-McAuley, Elaine Mitchell, Haotian Chen, Claire E. Widdicombe, Glen L. Wheeler, Richard G. Compton, Heather A. Bouman, and Rosalind E. M. Rickaby

Cite This: https://doi.org/10.1021/acsestwater.4c00530

Read Online

ACCESS | Metrics & More | Article Recommendations | Supporting Information

ABSTRACT: Phytoplankton are essential for the health of our oceans, yet existing *in situ* methods for monitoring phytoplankton abundance and community structure are limited, with relatively poor spatiotemporal coverage and taxonomic resolution, particularly among the nanoplankton size range. Here, we build on previous work and present field testing of a novel reagent-free fluoro-electrochemical technique for monitoring changes in nanoplankton abundance and community structure in natural seawater samples. This was achieved through the construction of a prototype sensor, which was then tested over a 3-month Spring−Summer period in 2023 with samples collected from the L4 station (Western English Channel). The measurements made by our sensor were successfully validated alongside microscope-based taxonomic enumerations and analytical flow cytometry. Of the phytoplankton functional groups of interest, our results demonstrate particularly strong correlations between the sensor and both microscope-based taxonomy and flow cytometry for enumerating small coccolithophorids (i.e., calcifying Isochrysidales, of the *Gephyrocapsa* genus) and between the prototype and microscope-based taxonomy for enumerating diatoms. We demonstrate that the inclusion of traditionally hard to identify nanoflagellates in our classifications has minimal effect on our ability to monitor overall shifts in community structure and bloom detection. Taking things forward, the potential for *in situ* deployment is discussed.

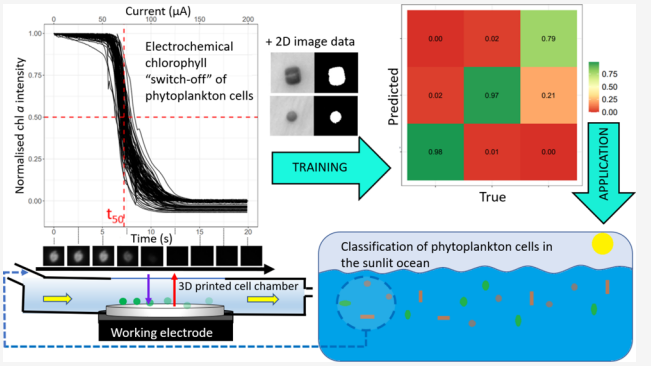

KEYWORDS: *ocean sensors, ocean monitoring, marine phytoplankton, nanoplankton, nanophytoplankton, electrochemical sensors, phytoplankton ecology*

INTRODUCTION

Unicellular phytoplankton play an integral role in the health of our oceans; they produce oxygen and fix the organic carbon that drives the biological carbon pump, while also functioning as the base of marine food webs, making them critical for biodiversity and ecosystem services. To better understand the impacts of climate change, and increased human impact on marine ecosystems, there is a pressing demand for high-resolution spatiotemporal monitoring of phytoplankton communities, which act as passive sentinels of change.[1] In particular, there is a need to quantify shifts in the abundance of ecologically relevant functional groups of phytoplankton, such as coccolithophores, diatoms, and dinoflagellates.[2] These groups have members that are bloom-forming, and their phenology typically reflects seasonal changes in environmental forcing. Gaining detailed insight into how such community dynamics are responding to a rapidly changing marine environment is therefore essential for understanding the broader ecological implications of climate change, along with assessing the direct side effects of anthropogenic activities. This is especially pertinent as new ventures seek to exploit the ocean for a variety of clean energy and net zero technologies, including growing interest in marine carbon dioxide removal (mCDR).[3]

Existing methods for monitoring *in situ* phytoplankton community structure and abundance have previously been summarized,[4] and include microscope-based taxonomy, flow cytometry, imaging flow cytometry, spectroscopy, and molecular techniques. While each method has its own merits,

Received: June 9, 2024
Revised: October 1, 2024
Accepted: October 3, 2024

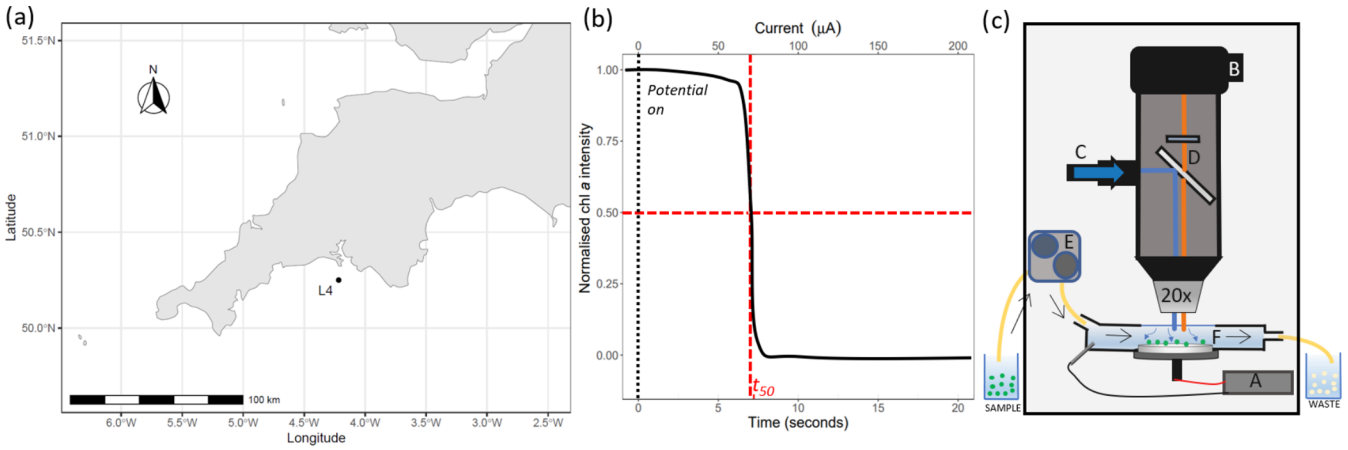

Figure 1. (a) Map of the UK's South West Peninsula, showing the location of the L4 sampling station in the Western English Channel. (b) Example of normalized Chl *a* fluorescence transient data for a single phytoplankton cell, following the onset of potential (at time 0 s, dotted black line) and with a current ramping of 10 μA s^{-1}. The dashed red markings highlight the time point, t_{50}, where normalized fluorescence values were reduced by 50%. (c) Simple schematic diagram of the prototype sensor (adapted from Barton et al. 2023), detailing the following components: custom-built galvanostat (A) connected to the working electrode (disc) and counter electrode (rod); camera (B); light-emitting diode (LED) input source (C); dichroic mirror and emission filter (D); peristaltic pump (E), for control of sample in, and waste out, with arrows indicating direction of flow; and three-dimensional (3D) printed electrochemical cell chamber (F), where phytoplankton settle by gravity onto the surface of the working electrode, allowing for the fluorescence of multiple cells to be monitored simultaneously. The optics are all part of a modular open-Frame microscope design, and all of the components listed above are housed inside a "black box", to aid prototype transport and to minimize contamination from stray light when making fluorescence measurements. Sample uptake and waste output tubes are fed into vials kept on the outside of the box (see Figure S1 for photographs of the prototype).

there are a number of trade-offs to be considered. Of relevance to this study is the ability to accurately quantify the abundance of cells belonging to relevant taxonomic or functional groups per unit volume seawater and the feasibility of high spatiotemporal resolution data collection. Microscope-based taxonomy is often considered the most accurate method for establishing the abundance of cells per unit volume, where in most cases, unicellular phytoplankton can be identified by a trained taxonomist at the genus and species level. In terms of spatiotemporal resolution, microscope taxonomy is limited: samples are collected at single points in space and time, and cells must be preserved with a fixative and left for >24 h to settle before identification and enumeration.[5] Flow cytometry provides rapid insight into community structure, and measurements can be obtained within minutes of obtaining both living and fixed samples from the environment. Cells can be grouped by clustering of light scattering and autofluorescence properties. This is particularly advantageous to distinguish cyanobacteria from eukaryotic phytoplankton within the picoplankton size range (<2 μm), and cryptophytes from the nanoplankton range (2−20 μm), due to their unique autofluorescence properties (driven by the presence of phycoerythrin). However, when it comes to distinguishing other ecologically relevant groups of the nanoplankton size fraction, only coccolithophores are quantifiable due to their unique light-scattering properties.[6−8] The emergence and continual development of imaging flow cytometry is a step forward in terms of categorizing plankton into ecologically relevant groups. These devices use a combination of images and cytometry measurements to classify marine microorganisms.[9] Importantly, they can be used *in situ*, either through ship-based deployment or on buoys;[10,11] thus, greatly enhancing the potential spatiotemporal resolution of measurements. Although it is evident that these devices perform well at the higher end of the phytoplankton size scale, *e.g.*, for microplankton (20−200 μm), the ability to classify accurately in the nanoplankton size range is somewhat limited by the resolution of images and the human input required to train the image-based machine learning.[12−17] To improve the characterization of the nanoplankton size fraction, previous studies often complement microscope taxonomy and cytometry analyses with molecular interpretations;[14,18] while this can offer improved taxonomic resolution, molecular insight only provides values for relative abundance, which can be subject to pronounced bias. Similarly, *in situ* hyperspectral measurements of particle absorption spectra can provide qualitative indications of the phytoplankton community structure through the detection of different chlorophyll pigments and phycoerythrin, but does not provide a quantitative indication of abundance.[19]

A recently introduced fluoro-electrochemical technique offers game-changing new opportunities for distinguishing cells into functional groups, with potential for autonomous *in situ* monitoring.[4,20−23] This reagent-free technique relies on controlled, electrochemically driven, oxidative destruction of cellular chlorophyll *a* (herein, Chl *a*) fluorescence over 10s of seconds in seawater samples, whereby the measured electrical charge required to "switch off" the Chl *a* fluorescence of an individual cell can be combined alongside basic properties of two-dimensional (2D) cell images (*e.g.*, effective cell radius) to classify cells. The key novelty of this approach comes from the differences in the relative susceptibility to oxidative stress across different phytoplankton functional groups. Using random forest machine learning, this method has demonstrated an excellent degree of accuracy when tested with >50 laboratory cultures of marine phytoplankton.[4] This prior work focused on the classification of nanoplankton, as it was identified that existing methods face more limitations when classifying phytoplankton in this size range. From previous studies of natural communities, in both coastal[24−28] and open ocean environments,[7,14,29,30] it is considered that nanoplankton can often dominate the phytoplankton biomass; with a large proportion of this size fraction being bulk classified by

https://doi.org/10.1021/acsestwater.4c00530
ACS EST Water XXXX, XXX, XXX−XXX

taxonomists as "nanoflagellates" or "phytoflagellates", when cells are similar in organic structure, and lack inorganic features for taxonomic identification.[28,31] Indeed, a long-term study of the pelagic phytoplankton community of the L4 station (Western English Channel, see Figure 1a), has demonstrated that on average, over a 15-year period, nanoflagellates can make up >80% of cell counts per unit seawater volume.[5] Taking this into account, for the fluoro-electrochemical technique to usefully categorize individuals into key functional groups, it must be able to minimize misidentification with this broad group of unknown nanoflagellates; or, even better, provide some indication of what these nanoflagellates might be. Flow cytometry also conducted on samples from the L4 station has only been able to monitor changes in the following groups of the nanoplankton fraction: coccolithophores, cryptophytes, and unknown nanoeukaryotes.[6,18] While preliminary work using the fluoro-electrochemical technique on laboratory cultures has demonstrated promising classification accuracy for key functional groups in the nanoplankton fraction,[4] a true test of its potential is validating its ability to quantify the abundance of functional groups in natural samples.

To this end, a portable prototype sensor was assembled and used to obtain fluoro-electrochemical measurements of the phytoplankton community structure from natural seawater samples collected at the aforementioned L4 station over a 3-month period during Spring−Summer 2023. This coincided with record high temperatures for June at the station, associated with a marine heatwave across the North Atlantic region.[32,33] Working with the nanoplankton size fraction specifically, we used our technique to classify unknown cells on a weekly basis to track changes in the abundance of key functional groups. This was validated against measurements obtained by microscope taxonomy (both conventional light microscopy and scanning electron microscopy), and cytometry for calcified cells. Two iterations of the validation were processed: one that classified cells based on the most abundant key functional groups that were found at L4: diatoms, dinoflagellates, and calcifying Isochrysidales (i.e., small coccolithophorids <10 μm ⌀, dominated by the *Gephyrocapsa* genus), and one that also included suspected nanoflagellates. We assessed the performance of the technique for monitoring the overall shift in the community over the 3-month period as well as a more detailed investigation of the classification performance of each group specifically.

MATERIALS AND METHODS

Electrochemical Technique and Prototype Sensor. The underlying electrochemical principles and methodology have been described in previous work.[4,21] In summary, phytoplankton cells deposited on the surface of a carbon electrode are exposed to an increasing concentration of oxidants in the seawater (hydrogen peroxide, hydroxyl radicals, hypobromous acid, dichlorine, and possible others), driven in a controlled manner by a constant ramping of electrical current using a galvanostat (in this work, 10 μA s^{-1}). As a result, a rapid decay of Chl *a* fluorescence of individual phytoplankton cells immobilized on the electrode is observed in the order of 10s of seconds (see Figure 1b); where the total electrical charge (driven by the constant ramping current), after time "t_{50}", required to switch off normalized Chl *a* fluorescence by 50% can be calculated for each cell.[21] The distinctive nature of this fluorescence decay, both in terms of half-life and the shape of the decay transient, has been demonstrated to be highly functional group specific.[4] In addition to the fluorescence imaging of Chl *a*, corresponding brightfield images of each individual are analyzed to derive secondary information about the 2D size and shape (*e.g.*, effective cell radius, aspect ratio, and circularity). A combination of both the charge at t_{50} and size and shape measurements can then be used to classify cell types against a trained "susceptibility library" derived from laboratory culture measurements.

To test the applicability of this method in classifying and enumerating unknown cells in natural seawater a custom-built semiautomated prototype sensor was developed (see Figures 1c, and S1). The design of the prototype follows a previous laboratory setup,[4,21] with a primary focus of mobility and low-power consumption, which are essential criteria for field testing purposes. Specifically, the electrochemistry was controlled by a galvanostat built using custom electronics. The body of the sensor was adapted from an open-source "open-Frame" microscope,[34] supplied by Cairn Research Ltd., U.K. A blue LED source (475 nm) was used, in conjunction with a dichroic mirror and emission filter (Filter Set 15, Carl Zeiss) to excite Chl *a* in fluorescence mode and allow wavelengths >590 nm range to be transmitted to a USB-powered camera (Blackfly S BFS-U3-89S6M, FLIR), and a 680 nm red LED source was also used to image cells in brightfield mode. For sample measurement, a variable-speed peristaltic pump was used to pass each sample through a shallow 3D-printed electrochemical cell chamber up to a maximum rate of 0.45 mL s^{-1}. Flow was stopped and started in a semicontinuous fashion to acquire data. When stopped, cells were deposited by gravity onto the carbon electrode, and fluoro-electrochemical data acquisition was initiated to obtain Chl *a* fluorescence "switch-off" profiles for each individual cell on the electrode surface. When flow through the cell chamber was resumed; waste material was pumped clear of the chamber and fresh sample was injected to repeat the process. The total number of fluoro-electrochemical acquisitions recorded was then used to calculate the total volume of the sample measured. All operation of the prototype was conducted using a Python-scripted interface. A small-form Odyssey computer (X86J4125800, Seeed Studio) which contains an integrated Arduino was used for the software-hardware communication via SPI (Serial Parallel Interface). The entire setup was designed to operate on a 12 V power supply. All fluorescence and brightfield images for each set of measurements were subsequently analyzed using ImageJ software (v1.53c, Fiji distribution).

Sample Collection and Preparation. Seawater was collected by Plymouth Marine Laboratory's RV Plymouth Quest from the L4 station on a weekly basis over a 3-month period, between April to June 2023. 20 L Niskin bottles were used to sample the water from a 10 m depth, and this was decanted into two 10 L carboys, which was brought to shore within 2−3 h of collection. Once in the laboratory (Marine Biological Association, Plymouth, U.K.) the seawater was gently filtered through a 30 μm nylon net (Merck Millipore Ltd.) to remove any zooplankton and microplankton, thus leaving nanoplankton of <30 μm in the filtrate. Given time constraints, all filtered seawater was then left overnight in controlled environment rooms that best represented the conditions at the time of sampling (based on CTD data) and on a 13:11 h light−dark cycle. The following morning the nanoplankton fraction was processed for various analyses

https://doi.org/10.1021/acsestwater.4c00530
ACS EST Water XXXX, XXX, XXX−XXX

within a 3−4 h period. Samples were preserved for conventional light microscope taxonomy and enumeration using two approaches: 250 mL was fixed with a final concentration of 1% Lugol's iodine solution and 200 mL was fixed with neutral formaldehyde (1% final concentration). The latter was necessary as Lugol's iodine solution contained ∼10% acetic acid, which results in the dissolution of extracellular calcite,[35] making calcifying nanoplankton unidentifiable. In addition, 400 mL was fixed with formaldehyde (1% final concentration) for scanning electron microscopy (SEM) based enumeration of calcified cell types; allowing more accurate identification based on coccolith morphology. These samples were stored in opaque bottles and refrigerated at 4 °C prior to taxonomic enumeration. A 1 mL aliquot of the live nanoplankton fraction was analyzed using a BD Accuri C6 benchtop flow cytometer (Becton Dickinson Ltd.) to specifically enumerate the abundance of viable calcified cells in the sample, distinguishable from other nanophytoplankton through their unique side-scatter signal. The cytometer was set to a medium speed (approximately 35 μL min^{-1}), and events were recorded over a 10 min period (resulting in approximately 342 μL of sample measured). We referred to Tarran and Bruun (2015) to determine the correct cytometry gating, as previously reported for coccolithophore abundance measurements at L4.

For use with the prototype sensor, 10 L of the <30 μm filtrate was concentrated to 100× by gently filtering through four 3 μm pore size, 45 mm ⌀, polycarbonate film track-etched membranes (Nuclepore, Whatman), using a vacuum pump and filtration manifold. Filtration was stopped when 25 mL seawater was remaining above each membrane in order to resuspend the concentrated residue and combine the concentrate from each to a final volume of 100 mL. Concentration was discovered to be a necessary step for running the prototype, to obtain a greater number of individual cells imaged per fluoro-electrochemical acquisition, and thus a higher throughput with time-sensitive live samples. It also resulted in the removal of picophytoplankton (cells <2 μm), which are typically unidentifiable by microscope taxonomy.

Conventional Light Microscope-Based Taxonomy and Enumeration. Nanoplankton samples fixed with 1% Lugol's iodine were identified to genus and species level using a 50 mL Utermöhl settling and counting chamber (Hydro-Bios, Germany). Well-mixed samples were poured into the chamber cylinder and left to settle out for 18−20 h, the cylinder was then exchanged with a coverslip, leaving behind 2.93 mL of sample containing the settled cells. The counting chamber was viewed on an inverted microscope (Axiovert S100, Carl Zeiss) using 200× and 400× magnification (the latter was used to locate fine structures) for taxonomic identification and enumeration. Once identified at genus and species level, cells were classified into the following functional groups: diatoms, dinoflagellates, ciliates, and nanoflagellates (the latter being allocated to the following subgroups: round <20 μm, round <10 μm, round <5 μm). Dinoflagellate enumeration included autotrophic, mixotrophic, and heterotrophic species.

For identification and enumeration of calcified cells, 100 mL of the 1% neutral formaldehyde preserved samples were prepared in counting chambers (as described above). After settling for >24 h, the concentrated samples were washed and dried to remove any residual formaldehyde. A Leica DMI4000B inverted microscope at 200× and 400× magnification, equipped with polarized and Differential Interference Contrast (DIC) filters, was used to identify and enumerate the calcified nanoplankton cells.[5] Unfortunately, due to issues with preservation, there were no enumerations of calcified cells using this method for 26th June.

SEM-Based Taxonomy and Enumeration. For the SEM-based taxonomy of calcified cells, 400 mL of the 1% formaldehyde-fixed nanoplankton fraction was passed through a 0.8 μm pore size, 25 mm ⌀ cellulose nitrate filter (Whatman) at a low vacuum pressure. Filters were dried in an oven at 60 °C for 6 h. A 0.5 cm square was cut from each filter and prepared on a 13 mm SEM stub (Agar Scientific, U.K.) for imaging using a low-vacuum environmental SEM (6390, JEOL Ltd.). A total of 500 fields of view were studied per sample at a magnification of 2000×, with intact calcified cells identified and counted cumulatively. From the total counts per 500 fields of view, assuming an even distribution of cells on the filter, the density of cells per unit volume was back calculated, as in refs 36−38. See Supporting Information for more extensive descriptions of all of the taxonomy procedures.

Training the Susceptibility Library for Natural Community Samples. In our previous work,[4] we presented a random forest machine learning-based approach for training and testing the classification accuracy of the technique using two predictor variables: charge at t_{50} (in mC) and effective cell radius (in μm). We have improved on this by including the following additional predictor variables, all of which can be derived from the 2D brightfield images of each cell using ImageJ: aspect ratio, circularity, Feret and minFeret (the maximum and minimum caliper diameters within the selected 2D cell shape boundary). The predictor variables were natural log-transformed prior to training the random forest with the R package "randomForest" (R version 4.2.2).

The data described above were collated for 38 strains from experimental measurements made in our previous study.[4] Within this data set, the following were identified as classifier groups of relevance for making comparisons against the grouped taxonomy enumerations (with the number of strains representing each group provided): diatoms (10), dinoflagellates (8), calcifying Isochrysidales (6), and nanoflagellates (14). For the latter, we speculated that nanoflagellates could belong to any of the following subgroups: Green algae (3), noncalcifying Isochrysidales (4), Pavlovales (3), Phaeocystales (1), and Prymnesiales (3). Each of these was included in the random forest, and the total of all of these made up the nanoflagellate group in the sensor-based enumerations. Given that the number of individual cells measured per strain differed substantially, to prevent skewing the representation of each group, cell numbers of each strain were randomly balanced to correspond with the strain of the lowest representation for each group (as described in ref 4). Given the reliance on Chl *a* fluorescence measurement, all dinoflagellates included in the training and testing were either autotrophic or mixotrophic. The number of individual measurements at the strain and group level and their average predictor variable values are summarized in Supporting Information Tables S1 and S2.

It is worth noting that no ciliates were included in the culture-based training and testing of the random forest, despite being observed in the taxonomy classifications. Subsequently, when it came to comparing classifications across both methods, ciliates were removed from the taxonomy data set. While this is a limitation of the approach, typically ciliates only made up between 0 and 1.2% of the total nanoplankton cell abundance.

https://doi.org/10.1021/acsestwater.4c00530
ACS EST Water XXXX, XXX, XXX−XXX

Furthermore, with the exception of 3 weeks during the field sampling where <0.01% of the total cells included in the taxonomy data set were identified as the coccolithophores *Coccolithus pelagicus* and *Acanthoica quattrospina*, all other calcified cells were identified as *Gephyrocapsa huxleyi*, reaching up to a maximum of 40% of the total nanoplankton community abundance across the weeks. The training of the random forest subsequently only included coccolithophorids belonging to the calcifying Isochrysidales order (with cell sizes <10 μm ⌀), of which the species *G. huxleyi* is typically considered the most globally abundant and ecologically relevant.[39,40]

Two iterations of the random forest training and testing were carried out to demonstrate classification accuracy; both without and with nanoflagellates included. This was relevant to determine whether additional confusion due to the inclusion of nanoflagellates hinders the classification of the key functional groups. In each case, training and testing were conducted with 80 and 20% subsets of strain data, respectively. In summary, following training, testing the random forest with just key groups included yielded an overall 95% accuracy, with F1 scores of 0.95 diatoms, 0.85 for dinoflagellates, and 0.98 for calcifying Isochrysidales (see Figure S2 and Table S3). When nanoflagellates were introduced, this resulted in a reduction of overall accuracy to 82%, and some reduction in F1 scores of the key groups; 0.84 diatoms, 0.82 for dinoflagellates, and 0.90 for calcifying Isochrysidales. There was a large variance in the performance across the suspected nanoflagellates, with F1 scores ranging from 0.84 (Pavlovales) to 0.25 (Green algae), see Figure S3 and Table S4. Following training and testing, 100% of the data for both iterations (without and with nanoflagellates, labeled throughout as v1 and v2, respectively) was then used for training the random forest to classify the data collected from the natural seawater samples.

Classification and Enumeration of Natural Samples. For each sampling date, 100 mL of the concentrated nanoplankton fraction was prepared. The concentrated sample was pumped into the 3D-printed cell chamber in a semicontinuous fashion, as described earlier. Each time the flow of the sample was stopped, 10 min was given to allow for deposition of the cells onto the electrode surface. Brightfield images of the cells in the microscopic field of view (647 μm × 341 μm) were initially obtained. Following this, fluorescence mode was activated, and cells were given an equilibrium period of 30 s to allow any natural Chl *a* fluorescence decay in response to the intense exposure to blue light, before the potential was applied using the galvanostat with a ramping current of 10 μA s^{-1}. Imaging was at the rate of 10 fps, and this ceased after a suitable period of time for all Chl *a* fluorescence in the field of view to be extinguished (10s of seconds). Throughout the field testing, an average of seven cells were measured simultaneously per fluoro-electrochemical acquisition. Following each acquisition, the sample chamber was pumped out for the next measurements.

Fluorescence transient data for each individual cell per image time series was processed as described in previous work, and a value for charge required to reach t_{50} was obtained.[4,21] In instances where there was significant movement of cells midtransient, these were voided from the data set to prevent erroneous t_{50} calculation. For each cell, the corresponding brightfield image was manually measured using ImageJ to derive the same predictor variables as described above for the training of the susceptibility library. Once the full data set was collated for each sample, the random forest iterations trained with 100% of the culture data (both with and without nanoflagellates—as described above) were used to classify each of the individual cells.

Sample abundance values (counts mL^{-1}) were derived by dividing the total number of cells classified in each group on each sampling date by the total sample volume measured. The total volume measured was estimated to be equivalent to the volume of seawater directly above the field of view, ranging from 0.176 to 0.309 μL (where the field of view is constant, as detailed above, and depth of the chamber between the electrode surface and the coverslip ranged between 800 and 1400 μm due to slight variance in the setup of the 3D sampling chamber on each sampling date), multiplied by the number of sequential semicontinuous fluoro-electrochemical acquisitions made for each sample (an average of 13 per concentrated sample on each date). This approach assumes that all cells belonging to the volume of seawater directly above the field of view were deposited on the electrode surface before each acquisition. Abundance values were then corrected to the original sample volume prior to concentration, with an average equivalent preconcentration sample volume of 0.324 mL (standard deviation (SD) ±0.11) across the sampling dates. In addition to absolute abundance, measurements of relative abundance can be highly useful for demonstrating shifts in community structure, regardless of the change in total cell numbers. Given that ciliates were removed from the original taxonomy data set and that we present two interpretations of the sensor-derived classifications to validate alongside microscope taxonomy (with and without nanoflagellates), we have calculated a proportion of those classified in each scenario. This is simply the counts mL^{-1} of each classified group presented as a percentage of the total count mL^{-1} for each specific date. To compare sensor-based measurements with taxonomic and cytometric enumerations, we obtained Pearson correlation coefficients (R) were obtained. To give an idea of sensitivity to high and low abundance throughout the testing period, we also report the maximum and minimum abundance values derived from each method (Table 1).

Artificial Intelligence: Neural Network Classification of Calcifying Isochrysidales. Our previous work has shown a particularly high degree of accuracy when using our technique to classify calcifying Isochrysidales, a group with remarkable resilience to the highly oxidative conditions relative to cells of comparable size.[4,23] To complement the output of the random forest machine learning, a one-dimensional (1D)-inception neural network was trained to use the full transient profiles of Chl *a* switch off (not just t_{50}), in combination with a simple measurement of effective radius, to classify calcifying Isochrysidales against all other types in the aforementioned susceptibility library. This approach also used 80% of the full data set for training and 20% for testing; obtaining an overall testing accuracy of 97.7%, and F1 scores of 0.98 for calcifying Isochrysidales and 0.96 for "other" (see Figures S4 and S5). Since the 1D-inception neural network achieved high accuracy on the testing data set, it was then applied to the field data to classify calcifying Isochrysidales from all other cell types. For a more extensive description, see Supporting Information.

RESULTS AND DISCUSSION

In this section, we present an overview of the phytoplankton community structure throughout the time series, reporting on both the taxonomy and sensor-based measurements. We then

https://doi.org/10.1021/acsestwater.4c00530
ACS EST Water XXXX, XXX, XXX−XXX

followed this up by examining the validation of the sensor measurements at the level of each functional group.

Overview of Taxonomy Findings. Taxonomy data at the genus and species level was separated into four main groups: diatoms, dinoflagellates, calcifying Isochrysidales, and nanoflagellates. The taxonomy work identified more than 50 different genera/species over the 3 months at L4, but only 3 of these species (*G. huxleyi*, *Prorocentrum micans*, *Prorocentrum minimum*) and only 5 genera (*Skeletonema*, *Thalassiosira*, *Amphidinium*, *Heterocapsa*, *Karenia*) were included in the culture-based training of the sensor. This highlights that any classification of cells into functional groups by the prototype sensor was reliant on the culture-based random forest being universally applicable to the much broader diversity found in natural samples.

Generally, the succession of the phytoplankton community over the Spring−Summer transition was as expected, based on previous long-term records of the L4 station,[5] see Figures 2a and 3a. Initially, nanoflagellates were most abundant, though this was soon followed by the arrival and dominance of the spring diatom bloom from mid- to late-April; largely associated with *Chaetoceros socialis*, *Pseudo-nitzschia seriata*, and *Thalassiosira* spp. Cell concentrations of diatoms rapidly declined in early May, followed by a marked increase in abundance of calcifying Isochrysidales (namely *G. huxleyi*, as confirmed by the SEM taxonomy, see Supporting Information) and a smaller peak of nanoflagellates. It is highly likely that this distinct shift in the community was related to an extended period of anticyclonic weather patterns in the study region from mid-May to June, bringing low wind speeds and high solar irradiance, resulting in increased stratification and sea surface temperatures over the period of study. This trend continued throughout June, and was subsequently categorized as a marine heatwave.[32,33] Such conditions, in addition to exhaustion of silicate concentration due to the earlier diatom bloom,[41] would have been favorable for *G. huxleyi* bloom formation, which peaked on 31st May in the taxonomy record. Dinoflagellate concentrations remained relatively low over the 3-month period (in the order of 10s of cells mL^{-1}), with a slight peak in numbers coinciding with the fall in diatoms and the increase in calcifying Isochrysidales. There was a second and less substantial peak in diatom abundance on 12th June; mainly consisting of *Leptocylindricus minimus* and *P. seriata* .

Overview of Sensor-Based Findings. When nanoflagellates were not included in the sensor classification, from a qualitative perspective, it is clear that the sensor performed well at capturing the general shifts in the community structure that were also seen in the taxonomic cell counts over the time series (see Figure 2b). There were notable differences in the absolute magnitude of cells mL^{-1} determined by the sensor

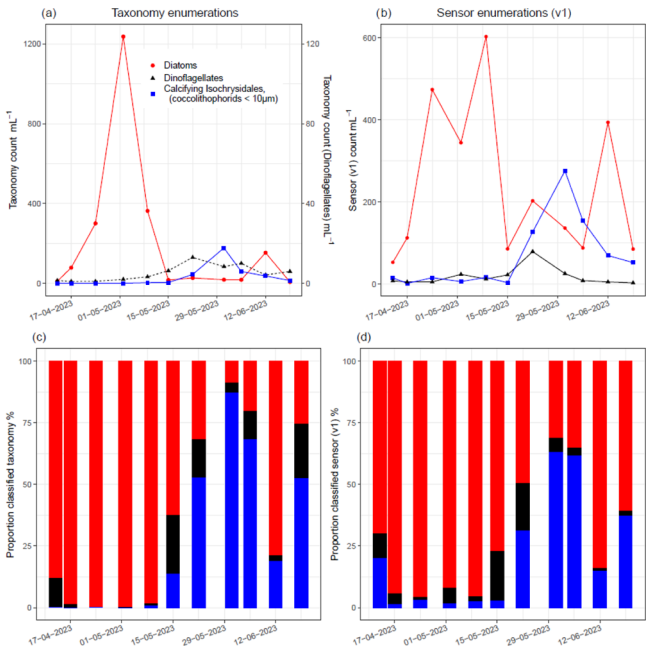

Figure 2. (a) Plot showing the abundance of the key functional groups enumerated by microscope-based taxonomy over the 3-month time series. The dashed line illustrates dinoflagellate counts to be read from the secondary *y*-axis, for visualization purposes. (b) The abundance of the key functional groups as measured using the prototype sensor over the time series, whereby nanoflagellates have been excluded from the random forest training (v1). (c) Bar plot showing the proportion of each of the key groups within the community, using classifications from the taxonomy data set with nanoflagellates excluded and (d) proportion of key groups in the community based on the measurements by the prototype sensor (v1). The color coding for (b)−(d) is the same as in (a). Due to poor preservation of the formaldehyde-fixed taxonomy samples taken on 26th June, it was not possible to present proportions of community abundance on this date. Therefore, to aid visual comparisons of community structure across the methods, data for 26th June was excluded from all plots in this figure.

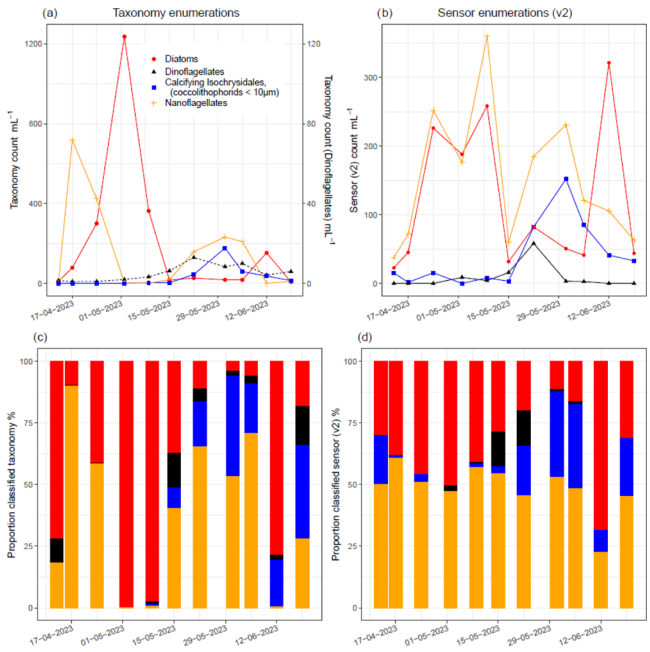

Figure 3. (a) Plot showing the abundance of the functional groups enumerated by microscope-based taxonomy over the 3-month time series, with nanoflagellates included. The dashed line illustrates dinoflagellate counts to be read from the secondary *y*-axis. (b) The abundance of the functional groups as measured by the prototype sensor over the time series, with nanoflagellates included in the random forest training (v2). (c) Bar plot showing the proportion of each of the groups within the community, using classifications from the taxonomy data set with nanoflagellates included (d) proportion of groups in the community based on the measurements by the prototype sensor (v2). The color coding for (b)−(d) is the same as in (a). Data for 26th June was excluded from all plots in this figure (see Figure 2 for explanation).

https://doi.org/10.1021/acsestwater.4c00530
ACS EST Water XXXX, XXX, XXX−XXX

(v1) for each of the groups, for example: the maximum calcifying Isochrysidales and dinoflagellate abundances were ∼1.5× and ∼6.1× greater than the taxonomic enumerations, and the maximum diatom numbers were ∼2.1× lower than the taxonomic enumerations. Despite these differences, it is promising that for the 3-month time series, the values of abundance were at least on the same order of magnitude for each group across the methods. On this point, the values derived by the sensor are also in a similar order of magnitude to the average values reported for diatoms, coccolithophorids (dominated by *G. huxleyi*) and dinoflagellates over the 15-year time series at L4, and follow similar seasonal trends previously observed.[5] Furthermore, the proportions of cells classified into each of the three key groups generally show the same pattern across the two methods, with diatoms dominating the community for the first 5 weeks, followed by an increasing proportion of calcifying Isochrysidales and dinoflagellates over the next 5 weeks throughout May and into June (see Figure 2c,d).

When nanoflagellates were included in the sensor classifications (v2) it did not drastically alter the patterns in community change seen across the time series; however, it did result in a reduction in the abundance values of the key functional groups, relative to the classifications without nanoflagellates considered (see Figure 3b). In relation to proportions of cells classified (Figure 3c,d), from a qualitative perspective, the addition of nanoflagellates appears to result in a time series that is in slightly less agreement with the taxonomy. Nonetheless, as nanoflagellates appear to remain in relatively high abundance throughout the time series, this somewhat agrees with previous long-term tracking of the L4 phytoplankton community, where there are less notable seasonal fluctuations in nanoflagellate abundance.[5]

Classification of Calcifying Isochrysidales (Coccolithophorids, <10 μm). Of the key functional groups monitored, the enumeration of calcifying Isochrysidales by the sensor was successfully validated by both microscope taxonomy and analytical flow cytometry. Figure 4a shows that all methods are consistent in capturing the entire bloom period, with all peak abundance values recorded on 31st May. The taxonomy counts were significantly correlated against both sensor counts (see Figure 4b,e, Table 1), with *R* values of >0.95, however, it is evident that when nanoflagellates were not included in training (v1) the sensor generally returned larger values than the taxonomy, whereas with nanoflagellates included in the training (v2) there was almost 1:1 correlation with the taxonomy values. For the latter, it is possible that the apparent lower abundance (relative to v1) is due to a proportion of calcifying Isochrysidales being classified as nanoflagellates, where testing of the random forest illustrated confusion with the following nanoflagellates; noncalcifying Isochrysidales and Pavlovales (see Figure S3). Furthermore, we found significant correlations between the taxonomy-defined proportion of abundance and that of both sensor-based measurements (see Figure 4d,g, Table 1).

In addition to the successful validation by microscope taxonomy enumerations, both sensor-based measurements yielded an even stronger agreement with flow cytometry enumerations of calcified cells (assumed to be entirely *G. huxleyi* given the dominance of this species in the SEM taxonomy record, see Supporting Information). This is particularly evident in the sensor iteration without nanoflagellates included (v1), where the correlation of abundance

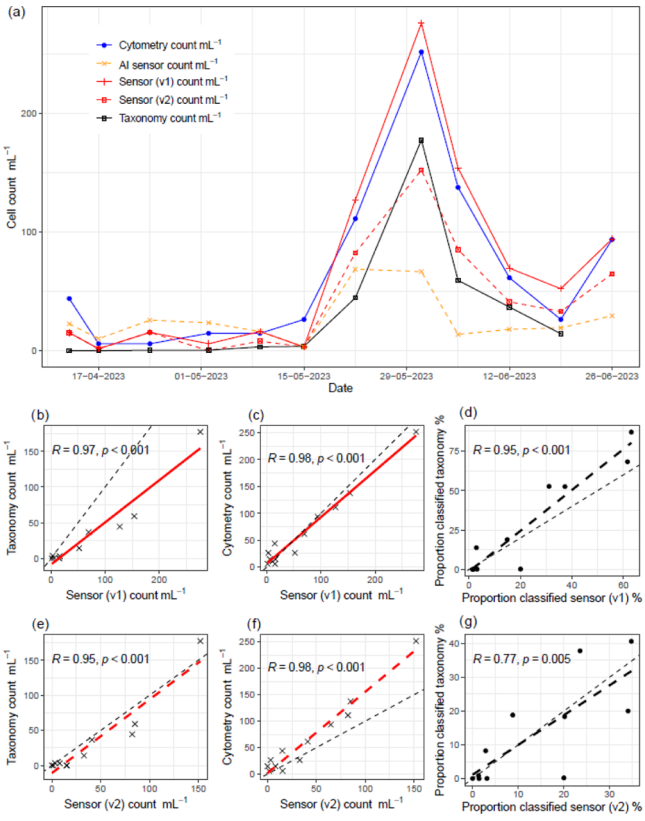

Figure 4. (a) Plot showing the abundance of calcifying Isochrysidales over the time series, as obtained through various methods. (b, e) Scatterplots showing the correlation between taxonomic counts and both sensor-based enumerations of calcifying Isochrysidales, without nanoflagellates v1 (b) and with nanoflagellates v2 (e) included in the random forest training. (c, f) Scatterplots showing the correlation between flow cytometry enumerations and both sensor-based enumerations, v1 (c) and v2 (f). (d, g) Scatterplots showing proportions of calcifying Isochrysidales in the nanoplankton community measured by taxonomic counts plotted against proportions obtained by the sensor, v1 (d) and v2 (g). The bold red and black lines (in b−g) represent signification correlation, as demonstrated by *R* and *p* values. The fine dashed-black lines represent the 1:1 line of the two measurements, in each instance.

values has an *R* of 0.98 ($p < 0.001$) (Figure 4c, Table 1), giving an excellent agreement with flow cytometry (almost 1:1). When nanoflagellates were included the correlation was equally as strong (Figure 4f, Table 1), however, the sensor produced values slightly lower than flow cytometry across most of the time series. It is highly probable that this reduction is simply due to an increased confusion with nanoflagellates, as mentioned above. While the SEM taxonomy usefully clarified that *G. huxleyi* was the dominant calcifier during the testing period, it is evident that the SEM-based cell counts were less accurate resulting in insignificant correlations with all other methods despite capturing the onset bloom (see Figure S6, Supporting Information). As can be seen from the methods for SEM enumeration, the process of preparing the formaldehyde-fixed samples has numerous steps, increasing the likelihood of losing intact cells. Perhaps most crucially, there is an assumption with the SEM method of uniform cell distribution across the filter surface used for SEM imaging, which could result in an erroneous back calculation of coccolithophore abundance in the original sample. On the other hand, both the prototype and cytometry measurements are obtained with live

https://doi.org/10.1021/acsestwater.4c00530
ACS EST Water XXXX, XXX, XXX−XXX

Table 1. Summary of the Regression Statistics for Each of the Cell Count Comparisons Presented in Figures 4−7[a]

Group	comparison ($x \sim y$)		R^2	R	p	Min. sensor (x)	Min. method (y)	Max. sensor (x)	Max. method (y)	Figure
calcifying Isochrysidales	sensor v1	taxonomy	**0.93**	**0.97**	**<0.001**	1.68	0.02	275.57	177.25	4b
	sensor v1	cytometry	**0.97**	**0.98**	**<0.001**	1.68	5.85	275.57	251.46	4c
	sensor v1%	taxonomy %	**0.89**	**0.95**	**<0.001**	1.41%	0.03%	63.04%	87.01%	4d
	sensor v2	taxonomy	**0.90**	**0.95**	**<0.001**	0	0.02	152.04	177.25	4e
	sensor v2	cytometry	**0.96**	**0.98**	**<0.001**	0	5.85	152.04	251.46	4f
	sensor v2%	taxonomy %	**0.59**	**0.77**	**0.005**	0%	0%	34.78%	40.64%	4g
diatoms	sensor v1*	taxonomy*	**0.91**	**0.95**	**<0.001**	52.84	6.98	602.58	362.99	5c
	sensor v1%	taxonomy %	**0.89**	**0.94**	**<0.001**	31.16%	8.88%	95.83%	99.81%	5d
	sensor v2*	taxonomy*	**0.67**	**0.82**	**0.002**	22.65	6.98	321.69	362.99	5f
	sensor v2%	taxonomy %	**0.49**	**0.70**	**0.016**	11.59%	4.15%	68.68%	99.60%	5g
dinoflagellates	sensor v1	taxonomy	**0.46**	**0.68**	**0.015**	2.75	0.94	78.92	13	6b
	sensor v1%	taxonomy %	**0.37**	**0.61**	**0.048**	1.04%	0.16%	20%	23.71%	6c
	sensor v2	taxonomy	**0.43**	**0.66**	**0.02**	0	0.94	58.33	13	6d
	sensor v2%	taxonomy %	0.14	0.38	0.248	0%	0.12%	14.29%	15.77%	6e
nanoflagellates	sensor v2	taxonomy	0.00	0.00	0.989	37.75	1.04	359.93	717.71	7b
	sensor v2%	taxonomy %	0.20	0.44	0.173	22.50%	0.20%	60.56%	90.04%	7c

[a]Minimum and maximum abundance values in counts mL^{-1} for both the sensor and other methods (either microscope-based taxonomy or flow cytometry enumerations) are provided to give an indication of performance at high and low abundances. Values presented as percentages are reflective of the maximum and minimum proportions of the community classified into each group. R is the Pearson correlation coefficient; bold text is used where the correlations considered significant (i.e., p value <0.05). * reflects the correlation following the removal of the data for 2nd May, as discussed in the text.

cells and with fewer stages of sample preparation; thus, making comparisons across these two techniques favorable. We might also expect that abundance of calcified cells will be more accurately established by the prototype (relative to other functional groups), given that deposition of cells on the electrode surface was necessary before measurements are made; this will have a natural bias toward accurate enumeration of cells that are ballasted by extracellular inorganic coatings, such as calcium carbonate coccospheres of coccolithophores and silica frustules of diatoms,[42] resulting in successful deposition of these cell types in the 3D-printed chamber.

Lastly, our 1D-inception neural network classifications (AI) resulted in statistically significant correlations with both the cytometry and taxonomy counts (Figures 4a and S6), however, the absolute abundance values were in closer agreement with the latter. The neural network interpretation of the prototype data was to simply classify calcifying Isochrysidales from all other cell types, using the full fluorescence transient data and a simple estimate of effective radius, as opposed to the broader suite of cell shape and size characteristics required with the random forest. It is promising that the period of maximal concentration could be detected from just the Chl *a* transient profile and a simple measure of cell size, illustrating the potential of artificial intelligence for making classifications with future versions of the technology.

Classification of Diatoms. The sensor-based classifications of diatoms tracked the taxonomy enumerations, indicating successful validation, with values that are comparable in magnitude across most of the time series (see Figure 5a). The biggest apparent mismatch with taxonomy is at the peak of the spring bloom on 2nd May. This outlier results in a nonsignificant correlation between the taxonomy and both iterations of the sensor measurements (see Figure 5b,e). However, based on the taxonomy findings, the most abundant diatom on this date was *C. socialis*, making up 98.2% of the diatom abundance, at a density of 1.2×10^4 mL^{-1} (which was the highest abundance value of any identified genera/species across the 3-month study). This is a chain-forming diatom, common in coastal areas, and under fast growth at high abundance it is highly plausible the chains were clumping and forming globular-spherical colonies.[43−45] While microscope taxonomy enumeration involved counting individual cells within the chains and colonies (which are likely to break up following addition of Lugol's, aiding the counting process), the fluorescence imaging of the sensor relies on single regions of fluorescence per cell. As a result, when such aggregates form, the fluorescence signals of individual cells can be harder to distinguish from one another, and thus colonies are poorly measured. Indeed, aggregates of cells were observed in the samples collected on May 2nd (see Figure S7). This raises questions about the applicability of the sensor in its current form, as it is likely to result in an erroneous abundance measurement when chain-forming nanodiatoms known to form such aggregates are in high abundance. Subsequently, it was demonstrated that when the highest abundance data for 2nd May was removed from the time series, both iterations of the sensor measurements result in a strong positive correlation with the taxonomy data, returning R values of 0.82 (p = 0.002) and 0.95 (p = <0.001) for classifications with (v2) and without (v1) nanoflagellates included (see Figure 5c,f, Table 1). In the case of the latter, there is greater deviation from the 1:1 line, suggesting that diatom abundance could be overclassified when nanoflagellates are excluded from the random forest training. Furthermore, when it comes to the proportion of diatoms classified within the nanoplankton community, correlations between both sensor interpretations and the taxonomy were also significant (see Figure 5d,g, Table 1).

Classification of Dinoflagellates. Dinoflagellates had the lowest abundance compared to the other classified groups, where the peak abundance was captured across all techniques on 22nd May, at 79 and 58 cells mL^{-1} for sensor measurements v1 and v2 respectively, and considerably lower at 13 cells mL^{-1} for the taxonomy (see Figure 6a, Table 1). The peak values derived from the sensor measurements are not too dissimilar to the long-term average dinoflagellate

https://doi.org/10.1021/acsestwater.4c00530
ACS EST Water XXXX, XXX, XXX−XXX

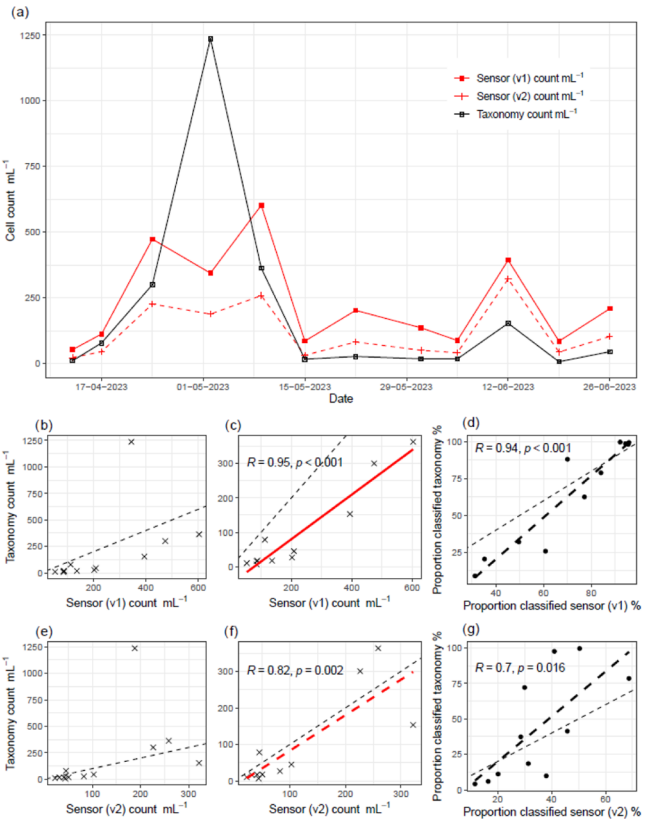

Figure 5. (a) Plot showing the abundance of diatoms over the time series, as obtained through various methods. (b, e) Correlation between taxonomy enumerations and both sensor-based enumerations of diatoms, without nanoflagellates v1 (b) and with nanoflagellates v2 (e) included in the random forest training. (c, f) Correlation between taxonomy enumerations and both sensor-based enumerations, v1 (c) and v2 (f), following the removal of the data for 2nd May, associated with high abundance of *C. socialis*. (d, g) Proportions of diatoms measured by taxonomy in the nanoplankton community plotted against proportions obtained by the sensor, v1 (d) and v2 (g). The bold red and black lines (in (c, d, f), and (g)) represent signification correlation, as demonstrated by *R* and *p* values. The fine dashed-black lines represent the 1:1 line of the two measurements in each instance.

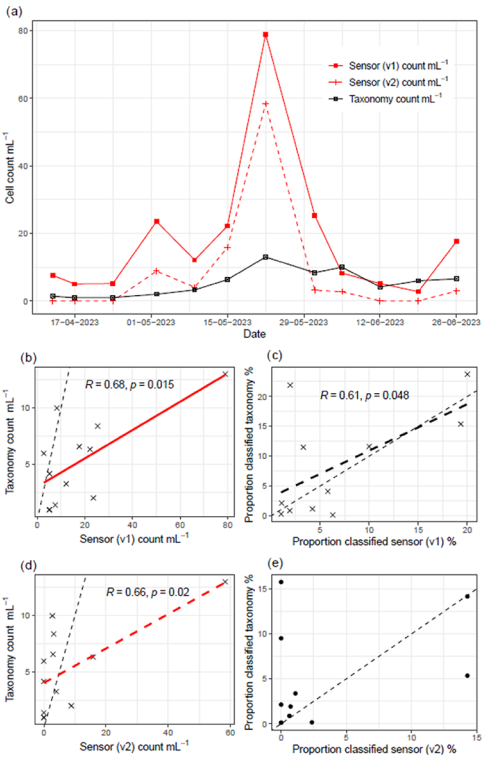

Figure 6. (a) Plot showing the abundance of dinoflagellates over the time series, as obtained through various methods. (b, d) Correlation between taxonomy enumerations and both sensor-based enumerations of dinoflagellates, without nanoflagellates v1 (b) and with nanoflagellates v2 (d) included in the random forest training. (c, e) Scatterplots showing proportions of dinoflagellates measured by taxonomy in the nanoplankton community plotted against proportions obtained by the sensor, v1 (c) and v2 (e). The bold red and black lines (in b–d) represent signification correlation, as demonstrated by *R* and *p* values. The dashed-black lines represent the 1:1 line of the two measurements, in each instance.

abundance of 81.9 cells mL^{-1} previously reported for L4.[5] Furthermore, the values throughout the rest of the time series (0–20 cells mL^{-1}) are roughly consistent with the seasonality of L4, where dinoflagellate numbers typically remain this low until late summer–early autumn, when concentrations can drastically increase and at times exceed 1000 cells mL^{-1}.[5] While the magnitude of the peak abundance over our study period differs substantially between both sensor measurements and the taxonomy, there is not much deviation between the values for the rest of the study period, resulting in marginally significant positive correlations between the taxonomy and sensor measurements (see Figure 6b,d, Table 1). There was also a marginally significant correlation between the proportion of dinoflagellates classified by taxonomy and the sensor interpretation without nanoflagellates, with minimal deviation from the 1:1 line, but not when nanoflagellates were included (Figure 6c,e, Table 1).

It might be expected that as most dinoflagellates are motile, a method that relies on cell deposition would struggle to detect them. It is therefore somewhat counterintuitive that the sensor measurements would suggest a greater peak abundance than taxonomy, which does not have the problem of motility due to the fixing of cells. It is highly plausible that the sensor misclassifies other cell types as dinoflagellates. Given that typical dinoflagellate abundance values are considerably lower during the testing months than the other functional groups,[5] any misclassification of other cell types as dinoflagellates would subsequently result in a much larger deviation from the taxonomy numbers. As opposed to if measurements were made during a dinoflagellate bloom, where the ratio of dinoflagellates to other cell types in the community would be much greater. Indeed, our random forest testing found dinoflagellates to be the hardest key functional group to classify, with the "without nanoflagellates" (v1) interpretation scoring 21% misclassification as diatoms, and the "with nanoflagellates" (v2) interpretation scoring 15% misclassification as nanoflagellates (Green algae and Prymnesiales) and 11% as diatoms (see Figures S2 and S3). It is also worth noting that a large proportion of dinoflagellates are heterotrophic, containing no plastid(s) or photosynthetic pigments.[46,47] A number of heterotrophic dinoflagellate species were identified at L4 by the microscope taxonomy, ranging between 21 and 65% of the total dinoflagellate abundance across the time series. Subsequently, these heterotrophs will not have been picked up by the sensor which relies on the Chl *a* fluorescence signal.

https://doi.org/10.1021/acsestwater.4c00530
ACS EST Water XXXX, XXX, XXX–XXX

However, if anything, this might result in a higher taxonomy count relative to the sensor, but that was not the case here. Moving forward, it must be stressed that only autotrophic and mixotrophic dinoflagellates can be classified with the sensor in its current form.

Classification of Nanoflagellates. From a methodological point of view, any sensor classification of nanoflagellates was based on assumptions of what genera, or species, might belong to this group of unknown cells that make up a significant proportion of phytoplankton communities in both the coastal and open ocean. As with our previous work,[4] we suggest that nanoflagellates could belong to any of the following: Green algae, noncalcifying Isochrysidales, Pavlovales, Phaeocystales, and Prymnesiales. These phytoplankton were selected in the classification training as there is often a great deal of similarity in cell morphology and a distinct lack of identifiable features to classify into any kind of taxonomic or functional grouping, particularly when in the lower end of the nanoplankton size range (<10 μm). Given such underlying assumptions, however, the sensor-based classifications into the nanoflagellate grouping could be considered highly speculative.

The abundance values of nanoflagellates classified across the study period fall into a similar range to the taxonomy (see Figure 7a), and the proportion of nanoflagellates within the nanoplankton community is also of a similar magnitude, though the overall correlation between values is poor relative to the other groups (see Figure 7b,c, Table 1). The only phase in the time series where there appears to be some clear correlation in values across the methods is between 15th and 31st May. Of the suspected nanoflagellate groups included in the training of the sensor, it appears that the initial peaks in nanoflagellate numbers (from mid-April to mid-May) are driven by the classification of both Prymnesiales and noncalcifying Isochrysidales, however, the later peak on 31st May appears to be largely driven by an increase in cells classified as Pavlovales (see Figure S8). We cannot read too much into this additional insight due to a lack of validation against taxonomy which would bulk label such cells as nanoflagellates. Only molecular analyses would be able to provide answers as to whether these speculated groups were present, and if there were any changes in their relative abundance over the time series.[14,29]

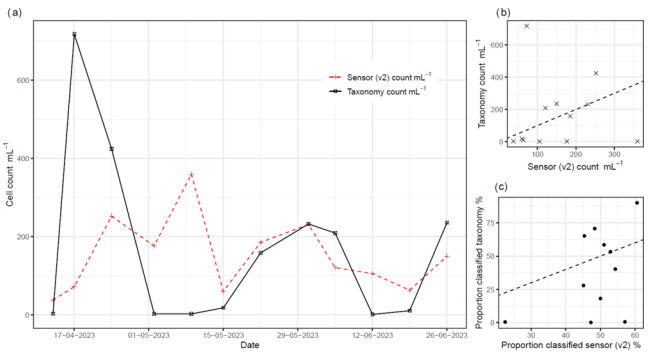

Figure 7. (a) Plot showing the abundance of nanoflagellates over the time series, as obtained through microscope-based taxonomy measurements and sensor measurements, whereby for the latter the nanoflagellate counts are the sum of all the cells classified as suspected nanoflagellate groups on each sampling date (see Figure S8). (b) Correlation between taxonomy enumerations and the sensor-based enumerations with nanoflagellates (v2) included in the random forest (c) scatterplot showing proportions of nanoflagellates measured by taxonomy in the nanoplankton community plotted against proportions obtained by the sensor (v2). The dashed-black lines represent the 1:1 line of the two measurements, in each instance.

Of particular curiosity is the fact that microscope taxonomy enumerations demonstrate the most abundant nanoflagellates across the time series to be those in the <5 μm size range, with this group driving the peaks observed across the time series. It is interesting that during the second peak of the nanoflagellates in the taxonomy record, between 15th May and 12th June, the abundance of small nanoflagellates (<5 μm) mirrors the cell counts of calcifying Isochrysidales from both the sensor and cytometry measurements samples (see Figure S9). It is highly plausible that in Lugol's iodine-preserved samples (with 10% acetic acid), the dissolution of coccospheres resulted in an apparent increase in abundance of small nanoflagellates, which could have in fact been *G. huxleyi* with their coccospheres removed (falling well within the <5 μm size range); it is well established that the underlying organic cell is still intact and measurable following such dissolution.[35,48,49] If this is the case with the Lugol's preserved samples, it has the potential to erroneously skew the concentrations of nanoflagellates found in the community by microscope taxonomy, particularly during a coccolithophore bloom.

Furthermore, if the second peak of nanoflagellates in the taxonomy records was due to the misclassification of decalcified *G. huxleyi* cells, then it raises the question as to why the sensor measured a similar second peak of nanoflagellates, largely driven by Pavlovales (see Figure S8). As mentioned previously, it is possible that a proportion of calcifying Isochrysidales are incorrectly identified as nanoflagellates, and this would explain the lower peak of calcifying Isochrysidales when nanoflagellates are included in the sensor classification (Figure 4a). Indeed, from testing the random forest with nanoflagellates included, the confusion matrix demonstrates a 5% misclassification of calcifying Isochrysidales as both Pavlovales and noncalcifying Isochrysidales, resulting in a reduction of the F1 score from 0.98 to 0.90 (see Figure S3 and Tables S3, S4). This is perhaps unsurprising, given that there is considerable overlap for a number of predictor variables across these classification groups (see Figure S10 and Table S2).

Outlook for *In Situ* Deployment. With rapidly changing marine environments, there is a growing need to improve the resolution of spatiotemporal monitoring of marine phytoplankton communities, particularly for those groups that drive the biological pump. This can only be achieved through the development and widespread deployment of *in situ* devices and sensors. The findings presented here demonstrate highly successful validation for the application of a fluoro-electrochemical sensor to distinguish and enumerate nanoplankton into groups of ecological relevance in natural seawater samples. For all groups classified in this study, the key shifts in community structure during the time series are consistent across the methods, as well as being in keeping with the expected trends for the L4 station.[5] Our sensor-based measurements have shown remarkable consistency when validated against both conventional microscope-based taxonomy and flow cytometry, whereby the latter is arguably the most comparable technique, allowing for differentiation and quantification of calcified cells from live nanoplankton samples. Unlike calcified cells, it is not possible to distinguish diatoms from other nanoeukaryotes using flow cytometry.[6,7] Therefore,

https://doi.org/10.1021/acsestwater.4c00530
ACS EST Water XXXX, XXX, XXX−XXX

a significant advancement of our technique over flow cytometry is that the fluoro-electrochemical sensor can provide realistic estimates of diatom abundance in the nanoplankton size range. The validation of the sensor for classifying dinoflagellates was less conclusive; however, the peak abundance was captured by both the sensor and the taxonomic enumerations. We can associate this with the timing of our field testing, where dinoflagellate abundance is typically at a low annual level at the L4 station. As a consequence, potentially erroneous misclassification of other cell types as dinoflagellates could have resulted in inflated numbers relative to the taxonomic enumerations. Lastly, when it comes to nanoflagellates, it is difficult to truly validate our method given the unknown identity of these cell types in the taxonomy record. While the abundance values were of a similar magnitude across the methods, the fluctuations across the time series were not as well synchronized (relative to the performance for other groups). Nonetheless, one of the most pertinent outcomes from the field testing is that by adding the potential confusion of nanoflagellates to the sensor-based enumerations, it does not drastically affect the ability of the sensor to successfully classify and capture the changes in community structure associated with the key functional groups.

Aside from the accurate classification of cells across different functional groups, there are numerous advantages of our technique that make it highly suitable for *in situ* deployment. The technique is reagent-free, relying solely on the oxidation of naturally occurring components in seawater to drive the fluorescence switch-off. In turn, the oxidative destruction of the phytoplankton cells means that the technique is intrinsically antifouling (at least in the vicinity of the working electrode, where the samples are measured); not dissimilar to the approach used to kill off invasive microbial species in ship's ballast water.[50−53] Furthermore, the majority of the components used to build the prototype are scalable and relatively inexpensive; highly favorable criteria from both a production and deployment perspective. With this in mind, a number of areas for improvement have been identified and should be considered for future development of the sensor, especially for compatibility with an autonomous platform. In its current form, the prototype requires samples to be concentrated in order to obtain a reasonable throughput of cells per measurement. Frequently in pelagic ecosystems nanophytoplankton abundance is in the order of 10s to 100s of cells mL^{-1}. Moving forward, to avoid the necessity to concentrate, it would be advantageous for the technique to obtain the fluoro-electrochemical measurements in a flow-type fashion (akin to flow cytometry); potentially using a series of in-flow ring electrodes, separated at regular intervals and applying different currents to track the fluoro-electrochemical Chl *a* switch-off of individual cells. Not only would this improve the throughput of measurements when cells are in low abundance but it would also remove any bias associated with settling times or lack of cell motility, as with the current design. To aid classification accuracy, additional variables could be measured at minimal adjustment to the setup to improve the random forest machine learning or expand neural network models. For example, the measurement of cell radius before and after the fluoro-electrochemical measurement would help to differentiate calcified cell types from others as well as potentially providing an estimate of calcite per cell, which would be highly useful for marine biogeochemists. This would be possible due to the intrinsic production of H^+ at the working electrode during the electrochemical measurements, which results in dissolution of coccospheres, as shown in our previous work.[35,48] In addition, if a broader suite of excitation and emission wavelengths were measurable then this could be used to further discriminate relevant groups of phytoplankton.[54] Notably, if there were a means to distinguish cells containing different pigments, such as chlorophyll *c* (common to those of a red algal lineage) from those containing chlorophyll *b* (common to those of a green algal lineage),[55,56] this could greatly assist in minimizing the large misclassifications observed between diatoms and green algae (see Figure S3). Lastly, only a relatively small number of species used for training the sensor were found at the L4 station. While this did not appear to impact the success of classifying key functional groups, expansion of nanoplankton diversity in the training data will likely improve the accuracy even further, increasing the likelihood of successful performance in different scenarios where community structure could be vastly different from that at L4. With this, future versions of the sensor should be tested over longer time scales in the field, ideally capturing a wider range of seasonal shifts in the nanophytoplankton community, and for multiple study locations where different environmental conditions and community compositions can be expected.

Ultimately, we envisage that our sensing method could be used to provide details of nanoplankton cell abundance and community structure that are currently lacking from most current *in situ* measurements, greatly adding to broader research efforts in understanding marine ecological responses to environmental change. Furthermore, as the technology has potential for deployment on autonomous platforms, if used in conjunction with a range of other "off-the-shelf" sensors to monitor key environmental variables (*e.g.*, pH, temperature, salinity), it could be invaluable for improving the spatiotemporal resolution of phytoplankton community monitoring at a global scale.

■ ASSOCIATED CONTENT

Supporting Information

The Supporting Information is available free of charge at https://pubs.acs.org/doi/10.1021/acsestwater.4c00530.

Photographs of the prototype sensor, detailed methods for microscope-based taxonomy and phytoplankton enumerations, culture library summary data and confusion matrices to illustrate the random forest and neural network testing, and additional figures to support the Results and Discussion sections (PDF)

Raw abundance values (XLSX)

■ AUTHOR INFORMATION

Corresponding Author

Samuel Barton − *Department of Earth Sciences, University of Oxford, Oxford OX1 3AN, U.K.;* orcid.org/0000-0003-2551-4297; Email: samuel.barton@earth.ox.ac.uk

Authors

Minjun Yang − *Physical and Theoretical Chemistry Laboratory, Department of Chemistry, University of Oxford, Oxford OX1 3QZ, U.K.; School of Chemistry, University of Leicester, Leicester LE1 7RH, U.K.;* orcid.org/0000-0001-8829-5883

Christopher Batchelor-McAuley − *School of Chemistry, Trinity College Dublin, Dublin 2, Ireland*

https://doi.org/10.1021/acsestwater.4c00530
ACS EST Water XXXX, XXX, XXX−XXX

Elaine Mitchell − *Scottish Association for Marine Science, Oban, Argyll PA37 1QA, U.K.*
Haotian Chen − *Physical and Theoretical Chemistry Laboratory, Department of Chemistry, University of Oxford, Oxford OX1 3QZ, U.K.;* orcid.org/0000-0003-1788-6605
Claire E. Widdicombe − *Plymouth Marine Laboratory, Plymouth PL1 3DH, U.K.*
Glen L. Wheeler − *Marine Biological Association, Plymouth PL1 2PB, U.K.*
Richard G. Compton − *Physical and Theoretical Chemistry Laboratory, Department of Chemistry, University of Oxford, Oxford OX1 3QZ, U.K.;* orcid.org/0000-0001-9841-5041
Heather A. Bouman − *Department of Earth Sciences, University of Oxford, Oxford OX1 3AN, U.K.*
Rosalind E. M. Rickaby − *Department of Earth Sciences, University of Oxford, Oxford OX1 3AN, U.K.*

Complete contact information is available at: https://pubs.acs.org/10.1021/acsestwater.4c00530

Author Contributions

Conceptualization: S.B., M.Y., C.B.-M., R.G.C., H.A.B., and R.E.M.R.; methodology: S.B., M.Y., C.B.-M., E.M., and C.E.W.; instrumentation: M.Y. and C.B.-M.; experiment: S.B.; analysis: S.B., M.Y., and H.C.; writing: S.B.; and review and editing: S.B., M.Y., C.B.-M., E.M., C.E.W., G.L.W., H.C., R.G.C., R.E.M.R., and H.A.B.

Notes

The authors declare no competing financial interest.

■ ACKNOWLEDGMENTS

This research was conducted with support from the Oxford Martin School Programme on Monitoring Ocean Ecosystems. The authors would like to thank the Electronics and Mechanical Workshops in the Oxford Chemistry Department for their help toward building this prototype. The authors also thank the crew and scientists of Plymouth Marine Laboratory's RV Plymouth Quest for their assistance with collection of seawater samples from Station L4, which forms part of the Western Channel Observatory and is funded by the UK Natural Environment Research Council through its National Capability Long-term Single Centre Science Programme, Climate Linked Atlantic Sector Science, grant number NE/R015953/1. The Marine Biological Association provided laboratory space and resources for testing the prototype.

■ REFERENCES

(1) Yang, M.; Compton, R. G. Electrochemical Sensors for Phytoplankton and Ocean Health. In *Current Opinion in Electrochemistry*; Elsevier B.V., 2023.
(2) Anderson, S. I.; Barton, A. D.; Clayton, S.; Dutkiewicz, S.; Rynearson, T. A. Marine Phytoplankton Functional Types Exhibit Diverse Responses to Thermal Change. *Nat. Commun.* **2021**, *12* (1), No. 6413.
(3) Boyd, P. W.; Claustre, H.; Legendre, L.; Gattuso, J.-P.; Le Traon, P.-Y. Operational Monitoring of Open-Ocean Carbon Dioxide Removal Deployments: Detection, Attribution, and Determination of Side Effects. *Oceanography* **2023**, *36* (1), 2−10.
(4) Barton, S.; Yang, M.; Chen, H.; Batchelor-McAuley, C.; Compton, R. G.; Bouman, H. A.; Rickaby, R. E. M. A Novel Fluoro-Electrochemical Technique for Classifying Diverse Marine Nanophytoplankton. *Limnol. Oceanogr.: Methods* **2023**, *21* (11), 656−672.
(5) Widdicombe, C. E.; Eloire, D.; Harbour, D.; Harris, R. P.; Somerfield, P. J. Long-Term Phytoplankton Community Dynamics in the Western English Channel. *J. Plankton Res.* **2010**, *32* (5), 643−655.
(6) Tarran, G. A.; Bruun, J. T. Nanoplankton and Picoplankton in the Western English Channel: Abundance and Seasonality from 2007−2013. *Prog. Oceanogr.* **2015**, *137*, 446−455.
(7) Tarran, G. A.; Heywood, J. L.; Zubkov, M. V. Latitudinal Changes in the Standing Stocks of Nano- and Picoeukaryotic Phytoplankton in the Atlantic Ocean. *Deep Sea Res., Part II* **2006**, *53* (14−16), 1516−1529.
(8) Collier, J. L. Flow Cytometry and the Single Cell in Phycology. *J. Phycol.* **2000**, *36* (4), 628−644.
(9) Lombard, F.; Boss, E.; Waite, A. M.; Uitz, J.; Stemmann, L.; Sosik, H. M.; Schulz, J.; Romagnan, J. B.; Picheral, M.; Pearlman, J.; Ohman, M. D.; Niehoff, B.; Möller, K. O.; Miloslavich, P.; Lara-Lopez, A.; Kudela, R. M.; Lopes, R. M.; Karp-Boss, L.; Kiko, R.; Jaffe, J. S.; Iversen, M. H.; Irisson, J. O.; Hauss, H.; Guidi, L.; Gorsky, G.; Giering, S. L. C.; Gaube, P.; Gallager, S.; Dubelaar, G.; Cowen, R. K.; Carlotti, F.; Briseño-Avena, C.; Berline, L.; Benoit-Bird, K. J.; Bax, N. J.; Batten, S. D.; Ayata, S. D.; Appeltans, W.; et al. Globally Consistent Quantitative Observations of Planktonic Ecosystems. *Front. Mar. Sci.* **2019**, *6*, No. 196.
(10) Dubelaar, G. B. J.; Gerritzen, P. L.; Beeker, A. E. R.; Jonker, R. R.; Tangen, K. Design and First Results of CytoBuoy: A Wireless Flow Cytometer for in Situ Analysis of Marine and Fresh Waters. *Cytometry* **1999**, *37* (4), 247−254.
(11) Olson, R. J.; Sosik, H. M. A Submersible Imaging-in-Flow Instrument to Analyze Nano-and Microplankton: Imaging FlowCytobot. *Limnol. Oceanogr.: Methods* **2007**, *5* (6), 195−203.
(12) Dugenne, M.; Thyssen, M.; Nerini, D.; Mante, C.; Poggiale, J. C.; Garcia, N.; Garcia, F.; Grégori, G. J. Consequence of a Sudden Wind Event on the Dynamics of a Coastal Phytoplankton Community: An Insight into Specific Population Growth Rates Using a Single Cell High Frequency Approach. *Front. Microbiol.* **2014**, *5*, No. 485.
(13) Fragoso, G. M.; Poulton, A. J.; Pratt, N. J.; Johnsen, G.; Purdie, D. A. Trait-Based Analysis of Subpolar North Atlantic Phytoplankton and Plastidic Ciliate Communities Using Automated Flow Cytometer. *Limnol. Oceanogr.* **2019**, *64* (4), 1763−1778.
(14) Bolaños, L. M.; Karp-Boss, L.; Choi, C. J.; Worden, A. Z.; Graff, J. R.; Haëntjens, N.; Chase, A. P.; Della Penna, A.; Gaube, P.; Morison, F.; Menden-Deuer, S.; Westberry, T. K.; O'Malley, R. T.; Boss, E.; Behrenfeld, M. J.; Giovannoni, S. J. Small Phytoplankton Dominate Western North Atlantic Biomass. *ISME J.* **2020**, *14* (7), 1663−1674.
(15) Chase, A. P.; Kramer, S. J.; Haëntjens, N.; Boss, E. S.; Karp-Boss, L.; Edmondson, M.; Graff, J. R. Evaluation of Diagnostic Pigments to Estimate Phytoplankton Size Classes. *Limnol. Oceanogr.: Methods* **2020**, *18* (10), 570−584.
(16) Fuchs, R.; Thyssen, M.; Creach, V.; Dugenne, M.; Izard, L.; Latimier, M.; Louchart, A.; Marrec, P.; Rijkeboer, M.; Grégori, G.; Pommeret, D. Automatic Recognition of Flow Cytometric Phytoplankton Functional Groups Using Convolutional Neural Networks. *Limnol. Oceanogr.: Methods* **2022**, *20* (7), 387−399.
(17) Irisson, J.-O.; Ayata, S.-D.; Lindsay, D. J.; Karp-Boss, L.; Stemmann, L. Machine Learning for the Study of Plankton and Marine Snow from Images. *Ann. Rev. Mar. Sci.* **2022**, *14*, 277−301.
(18) Stern, R.; Picard, K.; Clarke, J.; Walker, C. E.; Martins, C.; Marshall, C.; Amorim, A.; Woodward, E. M. S.; Widdicombe, C.; Tarran, G.; Edwards, M. Composition and Patterns of Taxa Assemblages in the Western Channel Assessed by 18S Sequencing, Microscopy and Flow Cytometry. *J. Mar. Sci. Eng.* **2023**, *11* (3), No. 480.
(19) Chase, A.; Boss, E.; Zaneveld, R.; Bricaud, A.; Claustre, H.; Ras, J.; Dall'Olmo, G.; Westberry, T. K. Decomposition of in Situ Particulate Absorption Spectra. *Methods Oceanogr.* **2013**, *7*, 110−124.

(20) Yang, M.; Batchelor-Mcauley, C.; Chen, L.; Guo, Y.; Zhang, Q.; Rickaby, R. E. M.; Bouman, H. A.; Compton, R. G. Fluoro-Electrochemical Microscopy Reveals Group Specific Differential Susceptibility of Phytoplankton towards Oxidative Damage. *Chem. Sci.* **2019**, *10* (34), 7988−7993.
(21) Yu, J.; Yang, M.; Batchelor-McAuley, C.; Barton, S.; Rickaby, R. E. M.; Bouman, H. A.; Compton, R. G. Rapid Opto-Electrochemical Differentiation of Marine Phytoplankton. *ACS Meas. Sci. Au* **2022**, *2* (4), 342−350.
(22) Yu, J.; Yang, M.; Batchelor-McAuley, C.; Barton, S.; Rickaby, R. E. M.; Bouman, H. A.; Compton, R. G. Does the Life Cycle Stage Matter for Distinguishing Phytoplankton via Fluoro-Electrochemical Microscopy? *Cell Rep. Phys. Sci.* **2023**, *4* (1), No. 101223.
(23) Chen, H.; Barton, S.; Yang, M.; Rickaby, R. E. M.; Bouman, H. A.; Compton, R. G. AI Facilitated Fluoro-Electrochemical Phytoplankton Classification. *Chem. Sci.* **2023**, *14* (22), 5872−5879.
(24) Barnes, M. K.; Tilstone, G. H.; Suggett, D. J.; Widdicombe, C. E.; Bruun, J.; Martinez-Vicente, V.; Smyth, T. J. Temporal Variability in Total, Micro- and Nano-Phytoplankton Primary Production at a Coastal Site in the Western English Channel. *Prog. Oceanogr.* **2015**, *137*, 470−483.
(25) Pinckney, J. L.; Benitez-Nelson, C. R.; Thunell, R. C.; Muller-Karger, F.; Lorenzoni, L.; Troccoli, L.; Varela, R. Phytoplankton Community Structure and Depth Distribution Changes in the Cariaco Basin between 1996 and 2010. *Deep Sea Res., Part I* **2015**, *101*, 27−37.
(26) Alves-De-Souza, C.; Benevides, T. S.; Santos, J. B. O.; Von Dassow, P.; Guillou, L.; Menezes, M. Does Environmental Heterogeneity Explain Temporal β Diversity of Small Eukaryotic Phytoplankton? Example from a Tropical Eutrophic Coastal Lagoon. *J. Plankton Res.* **2017**, *39* (4), 698−714.
(27) Leblanc, K.; Quéguiner, B.; Diaz, F.; Cornet, V.; Michel-Rodriguez, M.; Durrieu De Madron, X.; Bowler, C.; Malviya, S.; Thyssen, M.; Grégori, G.; Rembauville, M.; Grosso, O.; Poulain, J.; De Vargas, C.; Pujo-Pay, M.; Conan, P. Nanoplanktonic Diatoms Are Globally Overlooked but Play a Role in Spring Blooms and Carbon Export. *Nat. Commun.* **2018**, *9* (1), No. 953.
(28) Piwosz, K. Weekly Dynamics of Abundance and Size Structure of Specific Nanophytoplankton Lineages in Coastal Waters (Baltic Sea). *Limnol. Oceanogr.* **2019**, *64* (5), 2172−2186.
(29) Balzano, S.; Marie, D.; Gourvil, P.; Vaulot, D. Composition of the Summer Photosynthetic Pico and Nanoplankton Communities in the Beaufort Sea Assessed by T-RFLP and Sequences of the 18S RRNA Gene from Flow Cytometry Sorted Samples. *ISME J.* **2012**, *6* (8), 1480−1498.
(30) de Vargas, C.; Audic, S.; Henry, N.; Decelle, J.; Mahé, F.; Logares, R.; Lara, E.; Berney, C.; Le Bescot, N.; Probert, I.; Carmichael, M.; Poulain, J.; Romac, S.; Colin, S.; Aury, J.-M.; Bittner, L.; Chaffron, S.; Dunthorn, M.; Engelen, S.; Morard, R.; Mulot, M.; Scalco, E.; Siano, R.; Vincent, F.; Zingone, A.; Dimier, C.; Picheral, M.; Wincker, P.; Karsenti, E.; et al. Eukaryotic Plankton Diversity in the Sunlit Ocean. *Science* **2015**, *348* (6237), 1−12.
(31) McQuatters-Gollop, A.; Stern, R. F.; Atkinson, A.; Best, M.; Bresnan, E.; Creach, V.; Devlin, M.; Holland, M.; Ostle, C.; Schmidt, K.; Sheppard, L.; Tarran, G.; Woodward, E. M. S.; Tett, P. The Silent Majority: Pico- and Nanoplankton as Ecosystem Health Indicators for Marine Policy. *Ecol. Indic.* **2024**, *159*, No. 111650.
(32) McCarthy, G. D.; Plecha, S.; Charria, G.; Simon, A.; Poppeschi, C.; Russo, A. The Marine Heatwave West of Ireland in June 2023. *Weather* **2023**, *78* (11), 321−323.
(33) Berthou, S.; Renshaw, R.; Smyth, T.; Tinker, J.; Grist, J. P.; Wihsgott, J. U.; Jones, S.; Inall, M.; Nolan, G.; Berx, B.; Arnold, A.; Blunn, L. P.; Castillo, J. M.; Cotterill, D.; Daly, E.; Dow, G.; Gómez, B.; Fraser-Leonhardt, V.; Hirschi, J. J. M.; Lewis, H. W.; Mahmood, S.; Worsfold, M. Exceptional Atmospheric Conditions in June 2023 Generated a Northwest European Marine Heatwave Which Contributed to Breaking Land Temperature Records. *Commun. Earth Environ.* **2024**, *5* (1), No. 287.
(34) Lightley, J.; Kumar, S.; Lim, M. Q.; Garcia, E.; Görlitz, F.; Alexandrov, Y.; Parrado, T.; Hollick, C.; Steele, E.; Roßmann, K.; Graham, J.; Broichhagen, J.; McNeish, I. A.; Roufosse, C. A.; Neil, M. A. A.; Dunsby, C.; French, P. M. W. OpenFrame: A Modular, Sustainable, Open Microscopy Platform with Single-Shot, Dual-Axis Optical Autofocus Module Providing High Precision and Long Range of Operation. *J. Microsc.* **2023**, *292* (2), 64−77.
(35) Fan, X.; Batchelor-McAuley, C.; Yang, M.; Barton, S.; Rickaby, R. E. M.; Bouman, H. A.; Compton, R. G. Quantifying the Extent of Calcification of a Coccolithophore Using a Coulter Counter. *Anal. Chem.* **2022**, *94* (37), 12664−12672.
(36) Poulton, A. J.; Holligan, P. M.; Charalampopoulou, A.; Adey, T. R. Coccolithophore Ecology in the Tropical and Subtropical Atlantic Ocean: New Perspectives from the Atlantic Meridional Transect (AMT) Programme. *Prog. Oceanogr.* **2017**, *158*, 150−170.
(37) Charalampopoulou, A.; Poulton, A. J.; Tyrrell, T.; Lucas, M. I. Irradiance and PH Affect Coccolithophore Community Composition on a Transect between the North Sea and the Arctic Ocean. *Mar. Ecol.: Prog. Ser.* **2011**, *431*, 25−43.
(38) Charalampopoulou, A.; Poulton, A. J.; Bakker, D. C. E.; Lucas, M. I.; Stinchcombe, M. C.; Tyrrell, T. Environmental Drivers of Coccolithophore Abundance and Calcification across Drake Passage (Southern Ocean). *Biogeosciences* **2016**, *13* (21), 5917−5935.
(39) Bendif, E. M.; Probert, I.; Archontikis, O. A.; Young, J. R.; Beaufort, L.; Rickaby, R. E.; Filatov, D. Rapid Diversification Underlying the Global Dominance of a Cosmopolitan Phytoplankton. *ISME J.* **2023**, *17* (4), 630−640.
(40) Wheeler, G. L.; Sturm, D.; Langer, G. Gephyrocapsa Huxleyi (Emiliania Huxleyi) as a Model System for Coccolithophore Biology. *J. Phycol.* **2023**, *59* (6), 1123−1129.
(41) Smyth, T. J.; Fishwick, J. R.; Al-Moosawi, L.; Cummings, D. G.; Harris, C.; Kitidis, V.; Rees, A.; Martinez-Vicente, V.; Woodward, E. M. S. A Broad Spatio-Temporal View of the Western English Channel Observatory. *J. Plankton Res.* **2010**, *32* (5), 585−601.
(42) Durkin, C. A.; Van Mooy, B. A. S.; Dyhrman, S. T.; Buesseler, K. O. Sinking Phytoplankton Associated with Carbon Flux in the Atlantic Ocean. *Limnol. Oceanogr.* **2016**, *61* (4), 1172−1187.
(43) Pelusi, A.; Santelia, M. E.; Benevenuto, G.; Godhe, A.; Montresor, M. The Diatom Chaetoceros Socialis: Spore Formation and Preservation. *Eur. J. Phycol.* **2020**, *55* (1), 1−10.
(44) Sieracki, M. E.; Gifford, D. J.; Gallager, S. M.; Davis, C. S. Ecology of a Chaetoceros Socialis Lauder Patch on Georges Bank: Distribution, Microbial Associations, and Grazing Losses. *Oceanography* **1998**, *11* (1), 30−35.
(45) Smetacek, V. S. Role of Sinking in Diatom Life-History Cycles: Ecological, Evolutionary and Geological Significance. *Mar. Biol.* **1985**, *84*, 239−251.
(46) Hansen, P. J. Quantitative Importance and Trophic Role of Heterotrophic Dinoflagellates in a Coastal Pelagial Food Web. *Mar. Ecol.: Prog. Ser.* **1991**, *73*, 253−261.
(47) Hackett, J. D.; Anderson, D. M.; Erdner, D. L.; Bhattacharya, D. Dinoflagellates: A Remarkable Evolutionary Experiment. *Am. J. Bot.* **2004**, *91* (10), 1523.
(48) Yang, M.; Batchelor-McAuley, C.; Barton, S.; Rickaby, R. E. M.; Bouman, H. A.; Compton, R. G. Single-Entity Coccolithophore Electrochemistry Shows Size Is No Guide to the Degree of Calcification. *Environ. Sci.: Adv.* **2022**, *1* (2), 156−163.
(49) Yang, M.; Batchelor-McAuley, C.; Barton, S.; Rickaby, R. E. M.; Bouman, H. A.; Compton, R. G. Calcifying Coccolithophore: An Evolutionary Advantage Against Extracellular Oxidative Damage. *Small* **2023**, *19* (44), No. 2300346.
(50) Zhitao, Z.; Mindong, B.; Bo, Y.; Mindi, B.; Xiyao, B. Treatment of Invasive Marine Species on Board by Using Micro-Gap Discharge Plasma. *Plasma Sci. Technol.* **2005**, *7* (5), 3025−3029.
(51) Bai, M.; Zhang, Z.; Zhang, N.; Tian, Y.; Chen, C.; Meng, X. Treatment of 250 t/h Ballast Water in Oceanic Ships Using ·OH Radicals Based on Strong Electric-Field Discharge. *Plasma Chem. Plasma Process.* **2012**, *32* (4), 693−702.

https://doi.org/10.1021/acsestwater.4c00530
ACS EST Water XXXX, XXX, XXX−XXX

(52) Zhang, Y.; Bai, M.; Chen, C.; Meng, X.; Tian, Y.; Zhang, N.; Yu, Z. OH Treatment for Killing of Harmful Organisms in Ship's Ballast Water with Medium Salinity Based on Strong Ionization Discharge. *Plasma Chem. Plasma Process.* **2013**, *33* (4), 751−763.
(53) Lakshmi, E.; Priya, M.; Achari, V. S. An Overview on the Treatment of Ballast Water in Ships. *Ocean Coastal Manage.* **2021**, *199*, No. 105296.
(54) Zieger, S. E.; Seoane, S.; Laza-Martínez, A.; Knaus, A.; Mistlberger, G.; Klimant, I. Spectral Characterization of Eight Marine Phytoplankton Phyla and Assessing a Pigment-Based Taxonomic Discriminant Analysis for the in Situ Classification of Phytoplankton Blooms. *Environ. Sci. Technol.* **2018**, *52* (24), 14266−14274.
(55) Whatley, J. M.; Whatley, F. R. Chloroplast Evolution. *New Phytol.* **1981**, *87* (2), 233−247.
(56) Keeling, P. J. The Endosymbiotic Origin, Diversification and Fate of Plastids. *Philos. Trans. R. Soc., B* **2010**, *365*, 729−748.

https://doi.org/10.1021/acsestwater.4c00530
ACS EST Water XXXX, XXX, XXX−XXX